Published in final edited form as:
Int J Cancer. 2015 March 15; 136(6): 1321–1332. doi:10.1002/ijc.29094.

Runx2-Smad signaling impacts the progression of tumor-induced bone disease

Xuhui Zhang[1,2,‡], **Jacqueline Akech**[2], **Gillian Browne**[1,2], **Stacey Russell**[3], **John J. Wixted**[3], **Janet L. Stein**[1,2], **Gary S. Stein**[1,2], and **Jane B. Lian**[1,2,3,*]

[1]Department of Biochemistry, University of Vermont College of Medicine, Burlington, VT 05405

[2]Department of Cell Biology, University of Massachusetts Medical School, Worcester, MA 01655

[3]Department of Orthopedic Surgery and Rehabilitation, University of Massachusetts Medical School, Worcester, MA 01655

Abstract

Runx2, a master regulator of osteogenesis, is abnormally expressed in advanced prostate cancer. Here we addressed Runx2 contribution to formation of prostate cancer-related osteolytic and osteoblastic bone lesions by mediating TGFβ/BMP signaling through direct interaction with Smads. Further, we examined involvement of the Runx2-Smad complex in mediating tumor growth and distal metastasis. To identify Runx2-Smad specific mechanisms of prostate tumor activity in bone, we generated PC3 prostate cancer cell lines expressing Runx2-WT or one of two mutant proteins (Runx2-HTY and Runx2-ΔC) that each disrupt the Runx2-Smad interaction, either directly through a point mutation or by deletion of the functional C-terminus, respectively. Intratibial tumors generated from these cells revealed that Runx2-WT expressing cells resulted in predominantly osteolytic disease, while cells expressing mutant proteins exhibited tumors with mixed osteolytic/osteoblastic lesions. Extent of bone loss and of woven bone formation was assessed by radiography and micro-computed tomography. Bioluminescent imaging showed the presence of labeled prostate cancer cells in the lung at the latest time point examined, with Runx2-WT group exhibiting increased incidence of tumor cells in lung. Notably, disruption of the Runx2-Smad interaction significantly reduced incidence and size of lung tumors. Altered expression of Runx2 target genes involved in invasion, growth, adhesion and metastasis supported our findings. Thus, our studies demonstrate that Runx2 in prostate cancer cells plays a significant role in intratibial prostate cancer-related tumor growth and bone loss through mechanisms mediated by the Runx2-Smad signaling pathway. This work expands upon the potential importance of Runx2 as a therapeutic target in cancer.

Keywords

Runx2; prostate cancer; osteoblastic/osteolytic disease; metastatic bone disease; intratibial tumors

[*]Correspondence to: Jane B. Lian, Department of Biochemistry, University of Vermont College of Medicine, Burlington, VT 05405; F: 802-656-8216; jane.lian@uvm.edu.
[‡]Current address: Institute of Basic Medical Sciences, Beijing, 100850, China

Conflict of Interest Statement: None declared

Additional Supplementary Information may be found in the online version of this article.

Introduction

Prostate cancer is the most frequently diagnosed malignancy and the second leading cause of cancer-related death among men in the United States.[1] Prostate cancer bone metastasis is the leading cause of morbidity; almost 80% patients with advanced prostate cancer have bone metastasis.[2] While many factors have been associated with metastasis to bone, the osteogenic transcription factor Runx2 has been implicated in multiple stages of prostate cancer progression.[3,4] Runx2 is a scaffolding protein which promotes bone formation by interacting with regulators of cell growth (for example pRB, p53 and the WWOX tumor suppressor) or with mediators of signaling cascades that are upregulated in tumor cells, including TGFβ/BMP or Wnt in prostate tumor cells.[3,5] Runx2 is aberrantly expressed in advanced human prostate tumors and metastatic prostate cancer cell lines (e.g., PC3).[4] Past studies have indicated several regulatory factors in prostate tumors that result in highly expressed Runx2, including loss of miR-203, which represses Runx2,[6] as well as FOXO1, a negative regulator of Runx2.[7] Furthermore, many well characterized Runx2 target genes {e.g., vascular endothelial growth factor (VEGF), matrix metalloproteinases (MMPs), bone sialoprotein (BSP) and osteopontin (OPN)} are associated with tumor growth, invasion and metastasis to bone.[8–11] Transcriptome profiling of prostate cancer cells indicates that Runx2 upregulates multiple genes with prominent cancer associated functions.[12] Furthermore, Runx2 also increases survival of prostate cancer cells.[13] Recent evidence demonstrates that effective depletion of Runx2 by RNA interference inhibits migration and invasive properties of tumor cells and prevents metastatic bone disease.[4,14] Thus, characterizing the specific molecular properties contributing to these activities of Runx2 can lead to better therapeutic strategies.

Our previous studies have documented an important role of Runx2 in supporting osteolytic disease associated with breast and prostate tumor growth in bone.[4,14,15] Importantly, prostate tumors in bone generate mixed lesions with some osteolytic, but mainly osteoblastic, disease in which large amounts of woven bone are deposited from secreted tumor products and surrounding cells.[16,17] This pathologic bone formation occurs as a result of multiple molecular interactions among tumor, stromal, osteoclast and osteoblast lineage cells that are crucial in determining the extent of tumor growth and type of bone lesion.[16,18,19] TGFβ, a key bone matrix and tumor cell-derived factor, significantly contributes to osteolytic bone metastasis by regulating Smad2 and Smad3.[15,18–20] Numerous studies have documented that Runx2 mediates cellular responses to BMP/TGFβ signaling through formation of a Runx2-Smad transcriptional complex demonstrated by biochemical interaction and co-localization of the proteins in subnuclear domains.[21–24] The importance of the fidelity of Runx2-Smad interaction was first documented in a patient presenting with cleidocranial dysplasia, where a truncating nonsense mutation that impaired this interaction was identified.[25] Previously, a Smad interaction domain (SMID) was identified in the C-terminus of Runx2[21] and later the requirement of three amino acids (426–428, HTY) for functional activity in mediating TGFβ and BMP signaling in *in vitro* studies.[22] Mutation of these residues to AAA (designated Runx2-HTY) results in a protein that binds DNA to support transcriptional activity, but has impaired recruitment of Smad to Runx2 subnuclear foci.[22] The C-terminus of Runx2 is responsible for subnuclear targeting, as well as

transcriptional activation and repression.[26,27] The Runx2-ΔC mutant lacks the entire C-terminus of Runx2, and homozygous mice harboring a Runx2-ΔC mutation display neonatal lethality comparable to the Runx2-null mouse.[28] The presence of the SMID domain in the Runx2 C-terminus implicates the Runx2-Smad transcriptional complex as a key regulator of gene expression that promotes tumorigenesis and cancer-induced bone disease.

In this study, by using the Runx2–HTY mutant protein and the well documented intratibial model to study bone disease induced by tumor cells,[29] we could address the specific biological contribution of Runx2-Smad signaling in inducing bone lesions and metastasis. By expressing in PC3 cells WT Runx2 and two mutant proteins (described above) that disrupt Runx2-Smad signaling, and comparing to parental control cells, we have identified the contribution of the Runx2-Smad functional complex to tumor growth *in vivo*, the metastatic potential of tumors formed in bone, and changes in the extent of osteolytic versus osteoblastic disease. The mechanistic basis for these modifications due to impaired Runx2-Smad signaling is supported by a different profile of expressed genes among the cell lines. These findings, from both mutations, suggest novel targets of Runx2 related to different components of prostate tumor-induced bone disease.

Materials and Methods

Cell culture

For these studies, we used a sub-line of the PC3 advanced prostate cancer cell line that expresses endogenous Runx2 at low levels (PC3-L[4]; also designated PC3-2[17]) and was previously reported to result in mixed osteolytic and osteoblastic lesions.[4,17] Microsatellite analyses carried out by the Vermont Cancer Center DNA Analysis Facility verified the genotype as authentic PC-3 cells from ATCC. These cells were maintained in RPMI 1640 with 10% FBS and 10 mM non-essential amino acids, 2 mM L-glutamine, 1 mM sodium pyruvate, 100 U/ml penicillin and 100 μg/ml streptomycin. 293T cells were maintained in DMEM with 10% FBS and 2 mM L-glutamine, 100 U/ml penicillin and 100 μg/ml streptomycin. Media and supplements were obtained from Invitrogen (Grand Island, NY).

Adenovirus infection

Adenoviral delivery of vectors containing cDNA encoding Runx2-WT-IRES-GFP, Runx2-HTY-IRES-GFP, Runx2-ΔC-IRES-GFP under the control of the CMV5 promoter were used as described.[21] Preparation and purification of virus were performed using Adeno-X™ Maxi purification kit according to the manufacturer's protocols (Clontech, Mountain View, CA). For control of infection efficiency, the same adenovirus carrying GFP only was used. Cells were washed twice with serum-free medium after viral infection and cultured in regular medium for another 72 h before being harvested.

Lentivirus infection and cell sorting

For packaging, the lentiviral expression plasmids used were as follows: pLenti-DESTBLAST GFP (control), pLenti-DESTBLAST Runx2 WT–IRES-GFP, pLenti-DESTBLAST Runx2HTY(426–428AAA)-IRES-GFP and pLenti-DESTBLAST Runx2ΔC(C-terminal deletion mutant)-IRES-GFP. These plasmids were transfected into

293T cells using Lipofectamine 2000 (Invitrogen, Carlsbad, CA) according to manufacturer's instructions. After 48 h, 400 μl viral particles harvested from culture media were used for the infection of PC3-L cells in the presence of 4 μg/ml polybrene (Millipore, Billerica, MA). Infection efficiency (as monitored by evaluating cells expressing GFP by fluorescence microscopy) was ~50% before cell sorting by FACS (fluorescence activated cell sorting) to obtain pure populations that expressed GFP (95%). To obtain bioluminescent cells, PC3-L cells were first infected with lentivirus expressing a luciferase gene. Forty-eight hours later, the bioluminescent PC3 cells were seeded and further infected with lentiviruses expressing control GFP, Runx2-WT, and Runx2 mutant proteins (HTY and ΔC mutant).

Proliferation assay

Cell proliferation was assessed by cell counting. GFP, Runx2-WT, Runx2-HTY and ΔC mutant expressing PC3 cells were seeded in 12-well plates at a density of 1.5×10^4 cells. The number of cells was determined in three separate wells at days 1, 3 and 5 and in three independent experiments using the *Countess* cell counter (Life Technologies).

Western blot analysis

Cells were lysed in RIPA buffer with proteolytic inhibitors as previously described.[14] For western blot analysis, membranes were incubated with mouse anti-Runx2 monoclonal (1:1000, MBL, Woburn, MA), rabbit anti-GFP polyclonal (1:1000, Invitrogen, Carlsbad, CA) and rabbit anti-Cdk2 polyclonal antibody (1:5000, Santa Cruz Biotechnology, Dallas, TX) followed by HRP-conjugated goat anti-rabbit or goat anti-mouse secondary antibodies (Santa Cruz Biotechnology, Dallas, TX). Proteins were detected using Clarity™ Western ECL Substrate (Bio-Rad, Hercules, CA).

Quantitative reverse transcription-PCR

Total RNA was isolated from cells using Trizol reagent according to the manufacturer's protocol (Invitrogen) and then purified using a DNA-Free RNA kit (Zymo Research, Irvine, CA). cDNA was synthesized using Superscript First-Strand Synthesis System (Invitrogen). qRT-PCR was performed using SYBR Green Master Mix (Bio-Rad, Hercules, CA) and gene-specific primers (Table S1) in an ABI Prism 7000 thermocycler. Amplicon quantities were normalized to human Glyceraldehyde 3-phosphate dehydrogenase (GAPDH).

Animal protocols and histological analysis

Animal studies were conducted in accordance with approved Institutional Animal Care and Use Committee (IACUC) protocols and the NIH Guide for Care and Use of Laboratory Animals. Intratibial injections were performed as previously described.[4] Six severe combined immune-deficient (SCID) mice were used in each group. Tumors were allowed to grow for a period of 5 weeks. Bone lesions were analyzed weekly by radiography using the Faxitron MX-20 (Faxitron X-ray, Wheeling, IL). The area of osteolytic bone metastases visible on X-rays of tibias were quantified using ImageJ. For *in vivo* bioluminescence imaging, mice were administered 150 mg/kg dose of D-luciferin (Gold Biotechnology, St. Louis, MO) dissolved in PBS by intraperitoneal injection. Subsequently, mice were anesthetized using 2% isoflurane inhalation. To confirm distant metastatic foci,

bioluminescent signals present in the lung were measured. The tibia tumors were covered for the duration of this procedure to minimize signal interference from the tumor when measuring signal from the lungs.

For histological analysis, mice were sacrificed and both tumor-bearing tibias and contralateral limbs were excised for periodate-lysine-paraformaldehyde fixation (n=6 mice per group) for 72 h. Following μCT analyses, bones were decalcified in 18% EDTA (pH 7.4), and embedded in paraffin for Toluidine blue staining.[4,14]

Boyden chamber invasion assay

Cells (2.5×10^4) in serum-free RPMI 1640 (0.1% BSA) were seeded into the upper chamber of inserts containing membranes with 8μm pore size with or without Matrigel coating in a 24-well plate (BD Biosciences, San Jose, CA). Serum-containing growth medium was used in the bottom chamber as the attractant. After 24 h, the cells in the upper chamber were removed using a cotton swab, then fixed and stained with Hema-3 stain kit (Thermo Fisher Scientific, Waltham, MA) before counting cells using an inverted microscope. Wells were repeated in triplicate and the invaded/migrated cells were quantified per field of view and statistically analyzed. Data are expressed as the percent invasion through the Matrigel matrix and membrane relative to the migration through the control membrane.

Quantitation of bone mass and structure

Fixed bones were dehydrated in 70% alcohol for bone density and volume measurements, using the Scanco μCT 40 (Musculoskeletal Imaging Core, University of Massachusetts Medical School). Tibias were aligned axially and scanned at $70kV_p$, 114μA and a nominal resolution of 10 μm. The region of interest included 3 mm from the proximal growth plate of the tibia running distally. Images were reconstructed by Scanco software Version 5.0. For both the high and low density analyses, an $1866cm^2$ contour around the region of interest (excluding the fibula) was utilized. The segmentation parameters included the values 0.8 Gauss sigma, 1.0 Gauss support, a high density threshold of 250–1000 Hounsfield units (Hu) which measured high density bone in the range of 600–1200 mg of HA/cm^3) and a low density threshold of 175–275 for detecting low bone density in the range of <600mg of HA/$cm.^3$ As a reference for comparisons to the four test groups, the densities of the control tibia (contralateral tibia from n=3 mice) at high and low threshold were determined.

Statistical analysis

1Data were expressed as the mean ± standard error of the mean (SEM). Statistically significant differences between samples were determined using either the Student's t-test or ANOVA analyses as indicated. In all cases, $p<0.05$ was considered statistically significant.

Results

Generation of PC3 cell lines expressing Runx2 and mutant proteins

To identify the contribution of Runx2 to signaling that promotes tumor-induced bone disease through TGFβ in prostate cancer, we designed the Runx2-HTY mutant (426–428) to disrupt Runx2-Smad signaling, and the Delta C (ΔC) mutant in which the Runx2 C-terminus

(362–528) is deleted resulting in diminished transcriptional activity of Runx2 (see Fig. 1*a*). The previously characterized PC3-L cells[4,17] were selected for expression of the Runx2-WT and Runx2 mutant proteins because these cells produce mixed osteolytic and osteoblastic lesions analogous to human prostate metastatic bone disease, and thereby allow us to examine the contribution of the Runx2-Smad transcriptional complex to both arms of prostate-cancer induced bone disease. Furthermore, studies have shown that PC3 cell lines express multiple Smads.[24]

All the cell lines were sorted to enrich for expression of GFP and Runx2-WT and mutant proteins (Fig. 1*b*). Stable integration of Runx2-WT and both Runx2 mutant constructs is evidenced by protein expression up to 4 weeks post GFP sorting. We note that the empty vector GFP control has higher GFP expression when compared with others; this is likely due to the fact that only GFP is being expressed in the control, whereas Runx2 (and mutant proteins) as well as GFP - separated by an IRES sequence - are being translated from the same mRNA in the other cell lines.

mRNA analyses (qRT-PCR) showed that the Runx2-ΔC mutant expressing cells had higher Runx2 transcript levels (consistent with higher Runx2 protein) than either Runx2-WT or -HTY expressing cells (Figs. 1*b* and 1*c*). To address the transcriptional regulatory function of Runx2-WT and mutant proteins, we detected the expression of select established Runx2 target genes: colony stimulating factor 2 (CSF2) and osteopontin (OPN).[12,30] The increased mRNA levels of CSF2 and OPN (more than 14 fold and 4 fold, respectively) in Runx2-WT and Runx2-HTY overexpressing cell lines compared to the control GFP cells indicated functional Runx2 transcriptional activity (Fig. 1*c*). In contrast, the Runx2-ΔC mutant expressing cells appeared to lose most Runx2-mediated signaling pathway activities, as both CSF2 and OPN were detected at reduced levels compared to Runx2-WT group (Fig. 1*c*). This result is due to the altered functional properties of the Runx2-ΔC mutant which does not contain the C-terminal transcriptional activation domain, yet does retain the DNA binding domain. In summary, the PC3 cell sublines expressing the different Runx2 proteins used here showed stable Runx2 protein expression and with a consequent effect on Runx2 target genes compared to the control cells.

Runx2 protein variants modify the invasive ability of PC3 cells

To further investigate the phenotype of Runx2-WT and mutant expressing cell lines, *in vitro* invasive ability was examined (Figs. 2*a* and 2*b*). Representative images used to quantitate invasion rates are shown in Fig. 2*a*. All Runx2 expressing cells displayed an increased invasion rate compared with GFP expressing cells. Runx2-WT expressing cells exhibited the highest invasion ability (14%). Furthermore, cells expressing the Runx2-HTY and ΔC mutant proteins showed 40–50% lower invasion than the Runx2-WT protein expressing cells (Fig. 2*b*). To examine the effect of Runx2 on cell proliferation, cell numbers were counted over 5 days of logarithmic growth (Fig. 2*c*). Cell growth was not affected by the expression of Runx2-WT or Runx2-HTY; growth of the Runx2-ΔC mutant expressing cell line was significantly higher than Runx2-WT and Runx2-HTY expressing cells only at day 5 (Fig. 2*c*).

Overexpression of Runx2-WT and mutant proteins contributes to osteolytic bone disease

To investigate how exogenous expression of mutant Runx2 proteins compared to Runx2-WT affects tumor size, primary tumors in the tibias were monitored weekly following cell injection using the bioluminescent IVIS Imaging system (Supplementary Figure S2 shows mice in all experimental groups at weeks 1–5). Fig. 3*a* shows the typical tumor signal intensity in representative mice from all groups four weeks after injection. Fig. 3*b* shows the average total flux of the tumors over time derived from tumor luminescence. All mice in each group developed primary tumors within one week of injection. Tumors formed in the Runx2-ΔC group were significantly larger than the other three groups three, four and five weeks after injection ($p<0.05$). Histological sections of intratibial tumors confirmed overall tumor size at sacrifice (Fig. 3*c*). Consistent with *in vivo* imaging, the ΔC group had the largest tumors. The GFP, WT and ΔC groups exhibited very little trabecular bone, whereas the HTY group (which exhibited the least osteolysis, Fig. 3*d*) retained more trabecular bone (Fig. 3*c*).

Subsequently, to identify the functional activities of Runx2 in promoting bone lesions, PC3 cells expressing GFP, Runx2-WT, or -HTY or -ΔC mutants were injected into the intramedullary cavity of tibia in SCID mice. Three representative radiographs revealing osteolytic lesions present in tibia two weeks post-injection of each of the aforementioned cell lines are shown in Fig. 3*d*. Quantifying the area lacking trabecular bone in the radiographs (using ImageJ software) confirmed that the Runx2-WT group formed larger osteolytic lesions than the GFP, Runx2-HTY or -ΔC groups (Fig. 3*e*). These data indicate that the erosion area of the HTY group was lowest of all groups (Fig. 3*d & e*). The results demonstrate that disruption of Runx2-Smad signaling in the bone microenvironment modestly reduced the extent of osteolytic lesions.

Expression of WT Runx2 and mutant proteins influence tumor growth at distal sites

In vitro studies demonstrated increased invasive ability of prostate cancer cells expressing Runx2 proteins (Figs. 2*a* and 2*b*). Therefore, to address whether ectopic expression of Runx2 and Runx2 mutant proteins in PC3 cells influences their metastatic capacity, we examined the lungs of the same groups of mice presented in Fig. 3. By *in vivo* imaging of the lungs before sacrifice at the 5 week time point, we observed luminescence signals in the lung (shown in Fig. 4). No such signals were observed in the GFP control group (Figs. 4*a* and 4*b*), while 50% incidence of metastasis was evident in the Runx2-WT and -HTY mutant groups, but only 20% of the -ΔC group exhibited lung metastasis. Of further relevance, lung tumor growth was more pronounced in Runx2-WT compared to the HTY mutant (Figs. 4*a* and 4*c*) as reflected by total flux present in lung metastases being substantially higher for the WT group than the two groups expressing Runx2 mutant proteins (-HTY and -ΔC) (Fig. 4*c*). Although unlikely, authors cannot exclude the potential for unintended dissemination of tumor cells at the time of injection. However, taken together, these data allow us to deduce that expression of Runx2 proteins in prostate cancer cells injected into the tibia increased the propensity of tumor cells for distal metastasis. To further support this concept, the correlation of incidence and tumor size in the lung is consistent with tumor growth in bone (see Suppl. Figure 2 and Table S3). However, the ability of the cells to thrive in the distant

metastatic site appears to be due to the presence of the functional Runx2-Smad interacting domain.

Runx2 mutant proteins increase osteoblastic lesions in tumor bearing tibia

Because PC3 cells often result in mixed osteolytic and osteoblastic bone lesions, both of which are influenced by Smad signaling, we characterized the bone lesions induced by Runx2 expressing cells using micro-CT. Fig. 5*a* shows representative images of high density and low density bone from two mice per group (n=6). All groups exhibited values in a similar range for each type of bone density (Table S2). The high density bone (1000 ± 60 mg HA/cm^3) quantifies the percentage of normal bone remaining in the tumor bearing limb relative to the total volume area of the limb (bone volume fraction, percentage BV/TV, Fig. 5*b*). The volume of this fraction of bone in the area of tumor growth exhibited wide variation among the mice (n=6/group). A trend of high density bone volume for the HTY group was apparent when compared to GFP control and the Runx2-WT groups, while the ΔC group had the least high density bone (Fig. 5*b*). Although only moderate statistical significance was achieved (p=0.05, ANOVA), this observation suggests that the HTY group had the least osteolytic activity, and the ΔC group had the greatest amount of resorbed bone, confirming the radiographic findings (Fig. 3).

Subsequently, we evaluated the low density bone volume fraction (BV/TV), representing osteoblastic lesions caused by woven bone formation (Figs. 5*a* and 5*c*). This analysis revealed that there was a greater representation of osteoblastic lesions in the HTY and ΔC groups compared to the WT group. In contrast, the WT group exhibited the least amount of woven bone, consistent with and further supporting the notion from our earlier studies,[4,11] that Runx2 promotes osteolytic lesions (Fig. 3). A distinguishing feature of the Runx2 ΔC mutant was that it promoted bone resorption/osteolysis (Fig. 5*b*), but also stimulated more tumor growth with osteoblastic lesions (Figs. 3 and 5*c*). These bone density analyses have identified the contribution of the specific Smad signal to the type of bone lesion. Osteolytic lesions are more evident in Runx2-WT and -ΔC mice resulting in larger aggressive tumors than found in the Runx2-HTY mice; conversely, Runx2-HTY mice which exhibited the least tumor growth (Fig. 3) exhibited primarily osteoblastic disease. Moreover, the quantification of low density bone confirms that the loss of Runx2-Smad interaction in both the HTY and ΔC groups favors woven bone formation.

Disruption of Runx2-mediated signaling results in altered expression of genes related to tumor progression

To provide insight into potential mechanisms for the different functional activities of Runx2-WT and Runx2 mutant expressing cells, we examined a panel of genes that are either Runx2 targets and/or associated with osteolytic and/or osteoblastic disease (Figs. 6*a* and 6*b*). Expression of a number of osteolytic genes, including interleukin 11 (IL-11), parathyroid hormone-related protein (PTHrP)[4,14,31–33] and MMP2 (Fig. S1), was significantly increased in Runx2-WT expressing cells relative to the GFP control. However, IL-11 expression was reduced by 40% in Runx2-HTY and ΔC compared with Runx2-WT expressing cells. This finding suggests the Runx2-Smad interaction domain in the C-terminus is necessary for the regulation of IL-11 gene expression. PTHrP is also reduced in the Runx2-HTY compared

with -WT (2-fold), but Runx2-ΔC cells had 3 fold more expression than the Runx2-HTY mutant group (Fig. 6). OPG,[34] an inhibitor of osteoclastogenesis, exhibited increased expression in the Runx2-HTY and -ΔC mutants compared with the -WT cells. This gene expression profile is consistent with the differences in tumor size and the extent of resorption in the Runx2-ΔC and Runx2-HTY groups (Figs. 3 and 4*d*), with the high PTHrP level in Runx2-ΔC driving tumor growth, but OPG suppressing osteoclastic disease in favor of the osteoblastic lesions (Fig. 5).

Genes associated with tumor growth, osteoblastic lesions and metastasis showed striking differences among the groups (Fig. 6). VEGF has many activities, promoting angiogenesis, bone formation and metastasis.[35–37] The highest expression was found in the Runx2-HTY mutant, indicating that disruption of Runx2-Smad signaling can induce more osteoblastic-related gene expression. It is noteworthy that PAI-1, an inhibitor of tumor growth,[38] was present at very high levels in the Runx2-HTY expressing cells (4 fold compared to WT), while Runx2-ΔC had levels even lower than -WT, again correlating with opposing tumor size in these groups (Fig. 3). Fibronectin (FN1), which is linked to metastasis,[39] had high expression (4–5 fold) in both Runx2-WT and -HTY expressing cells as compared with other groups. This is consistent with the highest incidence of metastasis in the corresponding mice (n= 3/6, see Fig. 4) from the two groups. These gene expression patterns give insight at a mechanistic level in the context of cancer-induced bone disease to the observed properties of the PC3 cells expressing Runx2-WT, -HTY and -ΔC proteins, summarized in Fig. 6*c*. The gene expression analyses, together with the *in vivo* evidence for the distinct mouse phenotypes from each cell line, reveal the significant contribution of the Runx2-Smad pathway in Runx2-mediated tumor progression.

Discussion

Two novel and highly significant findings of the present study reveal the important contribution of the Runx2-Smad complex as a mediator of tumor-induced bone disease: Firstly, the disruption of Runx2-Smad alone through mutation of the Runx2-HTY interacting amino acids reduces tumor size and osteolytic bone disease; secondly, Runx2 is suggested to drive metastasis from bone to distal sites. For these studies, we used the prostate cancer PC3 cell line which we and others have reported exhibits mixed osteolytic-osteoblastic lesions, analogous to human metastatic bone disease in men.[4,16,17] By overexpressing Runx2-WT and two different mutants,[22] we could determine the contribution of Runx2 independent of Smad interactions and the Runx2-Smad complex to osteolytic and osteoblastic lesions. Our studies demonstrate that Runx2-Smad promotes the osteolytic process through regulation of IL-11 and PTHrP, as these two pathways are down-regulated by the Runx2-HTY mutant.

Consistent with the knowledge that Runx2 is abnormally and highly expressed in human prostate tumors at the late metastatic stage,[4,40,41] our data suggests that Runx2 is a mediator of metastasis to distal sites. Primary breast and prostate orthotopic tumors in the mouse do not metastasize to bone, and thus the intratibial injection model became widely used to study mechanisms of tumor cell activity within the bone microenvironment, resulting in cancer-cell induced bone disease. Importantly, the finding of luciferin-labelled cells in the lung after

5 weeks of advanced prostate tumor growth in bone, suggests the cells invaded the rich vasculature of bone tissue with lung being the primary distal site of subsequent metastasis in this model. Tumors arising from the control cells (GFP-only cells having low levels of Runx2[4]) showed no evidence of lung metastasis, while the Runx2-WT and Runx2-Smad mutant (Runx2-HTY) exhibited distal metastasis to lung (3/6 mice); however, Runx2-HTY mice had far less tumor growth activity at the lung distal site. In striking contrast, the Runx2-ΔC mutant, which exhibited robust tumor growth in bone, had very low incidence of metastasis (1/6). This mutant eliminates subnuclear targeting of Runx2 where functional transcriptional complexes are formed and deletes the activator and repressor functional domains.[26] The higher incidence of lung metastasis in the Runx2-HTY and WT groups can also be attributed to high levels of invasion-associated FN1[42] expression in cells used to form the tumors, as a contributing mechanism. Notably, the Runx2-ΔC group had lower FN1 levels and a lower incidence of metastasis.[4] Thus, these *in vivo* findings reveal that Runx2 may significantly impact metastasis to distal sites in prostate cancer.

Our studies have further identified mechanisms by which Runx2 and Runx2-Smad interactions mediate both osteolytic and osteoblastic disease. Osteolytic disease is well-established to result from the vicious cycle of TGFβ stimulated growth and tumor-secreted PTHrP promoting bone resorption.[18] Our earlier study established that Runx2 directly contributes to the osteolytic process by regulating the IHH-PTHrP pathway.[14] Here we demonstrated that uncoupling of the Runx2-Smad interaction significantly decreased the area of osteolytic bone disease (radiography) and tumor volume compared to WT. Thus, the decreased expression of PTHrP in cells expressing the Runx2-HTY mutant protein leads to decreased secretion of PTHrP *in vivo* and a consequent inhibition of the vicious cycle of resorption and tumor growth. Furthermore, Runx2-HTY cells have 50% reduced levels compared to WT of the resorptive cytokine IL-11, which was previously reported to be associated with osteolytic bone disease in highly metastatic breast cancer cells expressing endogenous Runx2.[43] In addition, the highest expression level of OPG, an inhibitor of osteoclastogenesis, is observed in these cells, adding a second arm to the inhibition of bone resorption. OPG is known to be inhibited by Runx2;[44] therefore, the two Runx2 mutants that disrupt Runx2-Smad signaling result in increased OPG that limits the extent of osteolytic disease from tumors formed in bone. Our studies identify that the Runx2 target genes OPG, VEGF, PAI-1, PTHrP and IL-11 are highly affected by Runx2-Smad signaling.

Disruption of the Runx2-Smad interaction significantly reduced tumor growth by blocking TGFβ-induced SMAD interaction with Runx2. Also contributing to the lowest tumor burden in the Runx2-HTY was the high expression of the TGFβ regulated gene PAI-1 that is an inhibitor of prostate tumor growth.[38] Of note, osteoblastic disease still occurred in the small tumors formed by the Runx2-HTY expressing PC3 cells, indicating that other factors contribute to woven bone formation in the tumors generated by these cells that do not require Runx2-Smad signaling. Previous studies have shown Wnt signaling contributes to the osteoblastic lesions.[16] Furthermore, VEGF, which has been reported to be a tumor growth and metastasis related factor,[36,37] was increased over controls in the Runx2-WT and -HTY expressing cells. VEGF is a direct target of Runx2 in bone,[45] and was recently described as a factor promoting bone formation,[46] thus potentially contributing to the

osteoblastic lesions in both Runx2-WT and -HTY groups. Thus, our data reveal that Runx2 upregulation of VEGF is dependent on Smad signaling. In conclusion, the gene expression profile, the smallest tumor size and least bone resorption in the Runx2-HTY group, all point to the significant contribution of Runx2-Smad mediated signaling in promoting prostate cancer induced bone disease. Contributing factors to the highest tumor volume observed in the Runx2-ΔC group likely include the low level of PAI1, as well as loss-of-function of Runx2 with co-regulatory factors. The Runx2-ΔC mutant eliminates subnuclear targeting of Runx2 where functional transcriptional complexes are formed and deletes activator and repressor functional domains.[26] Among the key co-regulatory factors is the spectrum of WW domain proteins forming a protein complex at the PPXY site with E3 ubiquitin ligases that target Runx2 to the proteasome.[47] Stimulated tumor growth by the Runx2-ΔC mutant may be a result of the highest expression levels of PTHrP found in this group (>15 fold). PTHrP is not only involved in the vicious cycle (described above), but is also associated with tumor growth[48] and osteoblast differentiation.[49] Therefore, the prolonged stimulation of osteoblast and osteoclast cells by PTHrP promotes the aggressive osteolysis as well as osteoblastic lesions observed in the Runx2-ΔC group. Interestingly, the CXCR4 chemokine protein[50] that promotes cell proliferation and tumor growth is also deregulated in the Runx2-ΔC group to a greater extent than WT. Thus, multiple molecular pathways, influenced by WT Runx2 in facilitating metastatic bone disease, have been identified.

In summary, each of the Runx2 mutants has revealed different responses of tumor cells in the bone microenvironment with respect to *in vivo* tumor growth, and formation of osteolytic and osteoblastic lesions and foci in lung supported by *in vivo* and *in vitro* mechanistic studies. Indeed, our data suggests that the Runx2-Smad signaling pathway in prostate cancer is a viable candidate for therapeutic targeting of tumor growth and associated bone disease complications.

Supplementary Material

Refer to Web version on PubMed Central for supplementary material.

Acknowledgments

We thank Sadiq Hussain (Department of Cell Biology, University of Massachusetts Medical School, Worcester, MA) for histology, and Jennifer Díaz for manuscript preparation. We thank members of the laboratory for stimulating discussions and support throughout the course of these studies.

Grant sponsor: National Institutes of Health; **Grant numbers**: P01 CA140043; R37 DE012528; P01 CA82834.

Abbreviations

VEGF	vascular endothelial growth factor
MMPs	matrix metalloproteinases
BSP	bone sialoprotein
OPN	osteopontin
SMID	Smad interaction domain

GAPDH	Glyceraldehyde 3-phosphate dehydrogenase
FBS	fetal bovine serum
IACUC	Institutional Animal Care and Use Committee
SCID	severe combined immune-deficient
Hu	Hounsfield units
SEM	standard error of the mean
ΔC	Delta C
qRT-PCR	mRNA analyses
CSF2	colony stimulating factor 2
BV	bone volume
TV	total volume
IL-11	interleukin 11
PTHrP	parathyroid hormone-related protein
FN1	Fibronectin
-HTY	-Smad mutant
WT	wild-type
RHD	runt homology domain
NLS	nuclear localization signal
BR	bone resorption
TG	tumor growth

References

1. American Cancer Society. Cancer Facts & Figures 2012. Atlanta: American Cancer Society; 2012. p. 68p
2. Rizzoli R, Body JJ, Brandi ML, Cannata-Andia J, Chappard D, El Maghraoui A, Gluer CC, Kendler D, Napoli N, Papaioannou A, Pierroz DD, Rahme M, et al. Cancer-associated bone disease. Osteoporos Int. 2013; 24:2929–2953. [PubMed: 24146095]
3. Pratap J, Lian JB, Stein GS. Metastatic bone disease: role of transcription factors and future targets. Bone. 2011; 48:30–36. [PubMed: 20561908]
4. Akech J, Wixted JJ, Bedard K, van der Deen M, Hussain S, Guise TA, van Wijnen AJ, Stein JL, Languino LR, Altieri DC, Pratap J, Keller E, et al. Runx2 association with progression of prostate cancer in patients: mechanisms mediating bone osteolysis and osteoblastic metastatic lesions. Oncogene. 2010; 29:811–821. [PubMed: 19915614]
5. Jiang Y, Dai J, Zhang H, Sottnik JL, Keller JM, Escott KJ, Sanganee HJ, Yao Z, McCauley LK, Keller ET. Activation of the Wnt pathway through AR79, a GSK3beta inhibitor, promotes prostate cancer growth in soft tissue and bone. Mol Cancer Res. 2013; 11:1597–1610. [PubMed: 24088787]
6. Viticchie G, Lena AM, Latina A, Formosa A, Gregersen LH, Lund AH, Bernardini S, Mauriello A, Miano R, Spagnoli LG, Knight RA, Candi E, et al. MiR-203 controls proliferation, migration and

invasive potential of prostate cancer cell lines. Cell Cycle. 2011; 10:1121–1131. [PubMed: 21368580]

7. Zhang H, Pan Y, Zheng L, Choe C, Lindgren B, Jensen ED, Westendorf JJ, Cheng L, Huang H. FOXO1 inhibits Runx2 transcriptional activity and prostate cancer cell migration and invasion. Cancer Res. 2011; 71:3257–3267. [PubMed: 21505104]
8. Lynch CC. Matrix metalloproteinases as master regulators of the vicious cycle of bone metastasis. Bone. 2011; 48:44–53. [PubMed: 20601294]
9. Gordon JA, Sodek J, Hunter GK, Goldberg HA. Bone sialoprotein stimulates focal adhesion-related signaling pathways: role in migration and survival of breast and prostate cancer cells. J Cell Biochem. 2009; 107:1118–1128. [PubMed: 19492334]
10. Tilli TM, Mello KD, Ferreira LB, Matos AR, Accioly MT, Faria PA, Bellahcene A, Castronovo V, Gimba ER. Both osteopontin-c and osteopontin-b splicing isoforms exert pro-tumorigenic roles in prostate cancer cells. Prostate. 2012; 72:1688–1699. [PubMed: 22495819]
11. Pratap J, Javed A, Languino LR, van Wijnen AJ, Stein JL, Stein GS, Lian JB. The Runx2 osteogenic transcription factor regulates matrix metalloproteinase 9 in bone metastatic cancer cells and controls cell invasion. Mol Cell Biol. 2005; 25:8581–8591. [PubMed: 16166639]
12. Baniwal SK, Khalid O, Gabet Y, Shah RR, Purcell DJ, Mav D, Kohn-Gabet AE, Shi Y, Coetzee GA, Frenkel B. Runx2 transcriptome of prostate cancer cells: insights into invasiveness and bone metastasis. Mol Cancer. 2010; 9:258. [PubMed: 20863401]
13. Lim M, Zhong C, Yang S, Bell AM, Cohen MB, Roy-Burman P. Runx2 regulates survivin expression in prostate cancer cells. Lab Invest. 2010; 90:222–233. [PubMed: 19949374]
14. Pratap J, Wixted JJ, Gaur T, Zaidi SK, Dobson J, Gokul KD, Hussain S, van Wijnen AJ, Stein JL, Stein GS, Lian JB. Runx2 transcriptional activation of Indian Hedgehog and a downstream bone metastatic pathway in breast cancer cells. Cancer Res. 2008; 68:7795–7802. [PubMed: 18829534]
15. Chen YC, Sosnoski DM, Mastro AM. Breast cancer metastasis to the bone: mechanisms of bone loss. Breast Cancer Res. 2010; 12:215. [PubMed: 21176175]
16. Sottnik JL, Keller ET. Understanding and targeting osteoclastic activity in prostate cancer bone metastases. Curr Mol Med. 2013; 13:626–639. [PubMed: 23061677]
17. Dutta A, Li J, Lu H, Akech J, Pratap J, Wang T, Zerlanko BJ, FitzGerald TJ, Jiang Z, Birbe R, Wixted J, Violette SM, et al. Integrin alphavbeta6 promotes an osteolytic program in cancer cells by upregulating MMP2. Cancer Res. 2014; 74:1598–1608. [PubMed: 24385215]
18. Weilbaecher KN, Guise TA, McCauley LK. Cancer to bone: a fatal attraction. Nat Rev Cancer. 2011; 11:411–425. [PubMed: 21593787]
19. Buijs JT, Stayrook KR, Guise TA. TGF-beta in the bone microenvironment: role in breast cancer metastases. Cancer Microenviron. 2011; 4:261–281. [PubMed: 21748439]
20. Padua D, Massague J. Roles of TGFbeta in metastasis. Cell Res. 2009; 19:89–102. [PubMed: 19050696]
21. Afzal F, Pratap J, Ito K, Ito Y, Stein JL, van Wijnen AJ, Stein GS, Lian JB, Javed A. Smad function and intranuclear targeting share a Runx2 motif required for osteogenic lineage induction and BMP2 responsive transcription. J Cell Physiol. 2005; 204:63–72. [PubMed: 15573378]
22. Javed A, Bae JS, Afzal F, Gutierrez S, Pratap J, Zaidi SK, Lou Y, van Wijnen AJ, Stein JL, Stein GS, Lian JB. Structural coupling of Smad and Runx2 for execution of the BMP2 osteogenic signal. J Biol Chem. 2008; 283:8412–8422. [PubMed: 18204048]
23. Lee KS, Kim HJ, Li QL, Chi XZ, Ueta C, Komori T, Wozney JM, Kim EG, Choi JY, Ryoo HM, Bae SC. Runx2 is a common target of transforming growth factor beta1 and bone morphogenetic protein 2, and cooperation between Runx2 and Smad5 induces osteoblast-specific gene expression in the pluripotent mesenchymal precursor cell line C2C12. Mol Cell Biol. 2000; 20:8783–8792. [PubMed: 11073979]
24. Gupta A, Cao W, Chellaiah MA. Integrin alphavbeta3 and CD44 pathways in metastatic prostate cancer cells support osteoclastogenesis via a Runx2/Smad 5/receptor activator of NF-kappaB ligand signaling axis. Mol Cancer. 2012; 11:66. [PubMed: 22966907]
25. Zhang YW, Yasui N, Ito K, Huang G, Fujii M, Hanai J, Nogami H, Ochi T, Miyazono K, Ito Y. A RUNX2/PEBP2alpha A/CBFA1 mutation displaying impaired transactivation and Smad

interaction in cleidocranial dysplasia. Proc Natl Acad Sci U S A. 2000; 97:10549–10554. [PubMed: 10962029]

26. Schroeder TM, Jensen ED, Westendorf JJ. Runx2: a master organizer of gene transcription in developing and maturing osteoblasts. Birth Defects Res C Embryo Today. 2005; 75:213–225. [PubMed: 16187316]
27. Zaidi SK, Sullivan AJ, van Wijnen AJ, Stein JL, Stein GS, Lian JB. Integration of Runx and Smad regulatory signals at transcriptionally active subnuclear sites. Proc Natl Acad Sci U S A. 2002; 99:8048–8053. [PubMed: 12060751]
28. Choi JY, Pratap J, Javed A, Zaidi SK, Xing L, Balint E, Dalamangas S, Boyce B, van Wijnen AJ, Lian JB, Stein JL, Jones SN, et al. Subnuclear targeting of Runx/Cbfa/AML factors is essential for tissue-specific differentiation during embryonic development. Proc Natl Acad Sci U S A. 2001; 98:8650–8655. [PubMed: 11438701]
29. Campbell JP, Merkel AR, Masood-Campbell SK, Elefteriou F, Sterling JA. Models of bone metastasis. J Vis Exp. 2012:e4260. [PubMed: 22972196]
30. Wai PY, Mi Z, Gao C, Guo H, Marroquin C, Kuo PC. Ets-1 and Runx2 regulate transcription of a metastatic gene, osteopontin, in murine colorectal cancer cells. J Biol Chem. 2006; 281:18973–18982. [PubMed: 16670084]
31. McCoy EM, Hong H, Pruitt HC, Feng X. IL-11 produced by breast cancer cells augments osteoclastogenesis by sustaining the pool of osteoclast progenitor cells. BMC Cancer. 2013; 13:16. [PubMed: 23311882]
32. Guise TA, Mohammad KS, Clines G, Stebbins EG, Wong DH, Higgins LS, Vessella R, Corey E, Padalecki S, Suva L, Chirgwin JM. Basic mechanisms responsible for osteolytic and osteoblastic bone metastases. Clin Cancer Res. 2006; 12:6213s–6216s. [PubMed: 17062703]
33. Lotinun S, Kiviranta R, Matsubara T, Alzate JA, Neff L, Luth A, Koskivirta I, Kleuser B, Vacher J, Vuorio E, Horne WC, Baron R. Osteoclast-specific cathepsin K deletion stimulates S1P-dependent bone formation. J Clin Invest. 2013; 123:666–681. [PubMed: 23321671]
34. Lacey DL, Boyle WJ, Simonet WS, Kostenuik PJ, Dougall WC, Sullivan JK, San Martin J, Dansey R. Bench to bedside: elucidation of the OPG-RANK-RANKL pathway and the development of denosumab. Nat Rev Drug Discov. 2012; 11:401–419. [PubMed: 22543469]
35. Kitagawa Y, Dai J, Zhang J, Keller JM, Nor J, Yao Z, Keller ET. Vascular endothelial growth factor contributes to prostate cancer-mediated osteoblastic activity. Cancer Res. 2005; 65:10921–10929. [PubMed: 16322239]
36. Bagri A, Berry L, Gunter B, Singh M, Kasman I, Damico LA, Xiang H, Schmidt M, Fuh G, Hollister B, Rosen O, Plowman GD. Effects of anti-VEGF treatment duration on tumor growth, tumor regrowth, and treatment efficacy. Clin Cancer Res. 2010; 16:3887–3900. [PubMed: 20554752]
37. Karnezis T, Shayan R, Caesar C, Roufail S, Harris NC, Ardipradja K, Zhang YF, Williams SP, Farnsworth RH, Chai MG, Rupasinghe TW, Tull DL, et al. VEGF-D promotes tumor metastasis by regulating prostaglandins produced by the collecting lymphatic endothelium. Cancer Cell. 2012; 21:181–195. [PubMed: 22340592]
38. Jorgenson E, Deitcher SR, Cicek M, Liu X, Plummer S, Casey G, Witte JS. Plasminogen activator inhibitor type-1 (PAI-1) polymorphism 4G/5G is associated with prostate cancer among men with a positive family history. Prostate. 2007; 67:172–177. [PubMed: 17044080]
39. Pal S, Ganguly KK, Chatterjee A. Extracellular matrix protein fibronectin induces matrix metalloproteinases in human prostate adenocarcinoma cells PC-3. Cell Commun Adhes. 2013; 20:105–114. [PubMed: 24047237]
40. Yun SJ, Yoon HY, Bae SC, Lee OJ, Choi YH, Moon SK, Kim IY, Kim WJ. Transcriptional repression of RUNX2 is associated with aggressive clinicopathological outcomes, whereas nuclear location of the protein is related to metastasis in prostate cancer. Prostate Cancer Prostatic Dis. 2012; 15:369–373. [PubMed: 22890388]
41. Brubaker KD, Vessella RL, Brown LG, Corey E. Prostate cancer expression of runt-domain transcription factor Runx2, a key regulator of osteoblast differentiation and function. Prostate. 2003; 56:13–22. [PubMed: 12746842]

42. Jia D, Entersz I, Butler C, Foty RA. Fibronectin matrix-mediated cohesion suppresses invasion of prostate cancer cells. BMC Cancer. 2012; 12:94. [PubMed: 22433434]
43. Mendoza-Villanueva D, Zeef L, Shore P. Metastatic breast cancer cells inhibit osteoblast differentiation through the Runx2/CBFbeta-dependent expression of the Wnt antagonist, sclerostin. Breast Cancer Res. 2011; 13:R106. [PubMed: 22032690]
44. Enomoto H, Shiojiri S, Hoshi K, Furuichi T, Fukuyama R, Yoshida CA, Kanatani N, Nakamura R, Mizuno A, Zanma A, Yano K, Yasuda H, et al. Induction of osteoclast differentiation by Runx2 through receptor activator of nuclear factor-kappa B ligand (RANKL) and osteoprotegerin regulation and partial rescue of osteoclastogenesis in Runx2−/− mice by RANKL transgene. J Biol Chem. 2003; 278:23971–23977. [PubMed: 12697767]
45. Zelzer E, Glotzer DJ, Hartmann C, Thomas D, Fukai N, Soker S, Olsen BR. Tissue specific regulation of VEGF expression during bone development requires Cbfa1/Runx2. Mech Dev. 2001; 106:97–106. [PubMed: 11472838]
46. Liu Y, Berendsen AD, Jia S, Lotinun S, Baron R, Ferrara N, Olsen BR. Intracellular VEGF regulates the balance between osteoblast and adipocyte differentiation. J Clin Invest. 2012; 122:3101–3113. [PubMed: 22886301]
47. Bae SC, Lee YH. Phosphorylation, acetylation and ubiquitination: the molecular basis of RUNX regulation. Gene. 2006; 366:58–66. [PubMed: 16325352]
48. Li J, Karaplis AC, Huang DC, Siegel PM, Camirand A, Yang XF, Muller WJ, Kremer R. PTHrP drives breast tumor initiation, progression, and metastasis in mice and is a potential therapy target. J Clin Invest. 2011; 121:4655–4669. [PubMed: 22056386]
49. Martin TJ. Osteoblast-derived PTHrP is a physiological regulator of bone formation. J Clin Invest. 2005; 115:2322–2324. [PubMed: 16138187]
50. Luker KE, Lewin SA, Mihalko LA, Schmidt BT, Winkler JS, Coggins NL, Thomas DG, Luker GD. Scavenging of CXCL12 by CXCR7 promotes tumor growth and metastasis of CXCR4-positive breast cancer cells. Oncogene. 2012; 31:4750–4758. [PubMed: 22266857]

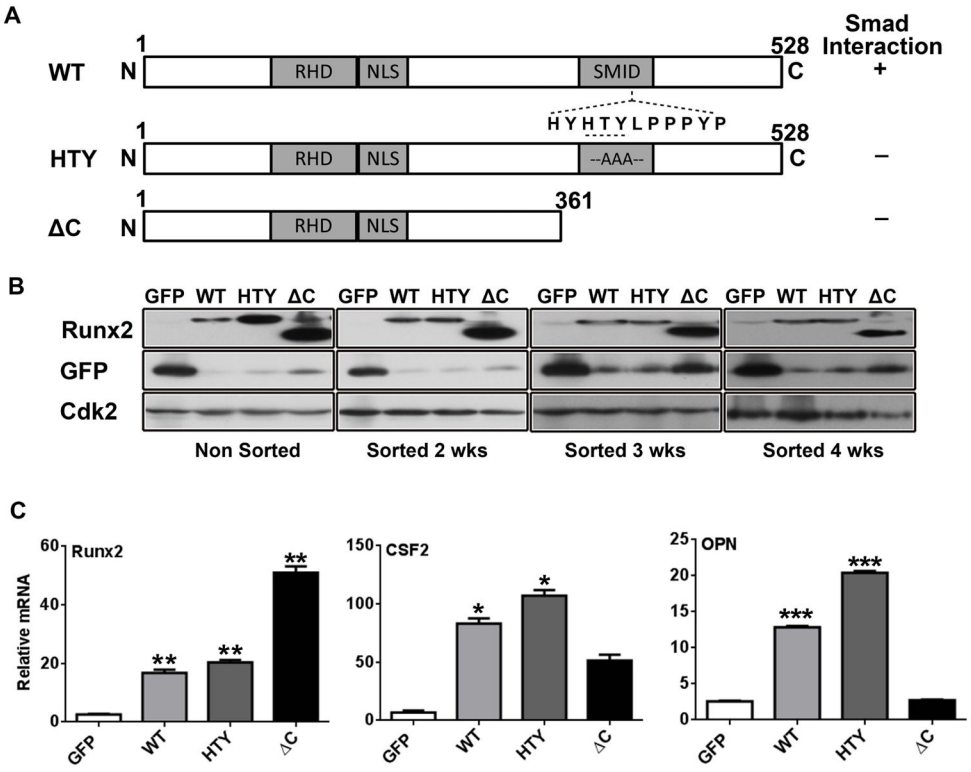

Figure 1.

Generation of PC3 cell lines expressing Runx2 and Runx2 mutant proteins. (*A*) Schematic illustration of the wild-type (WT) and mutant Runx2 (HTY: three essential amino acids mutated to AAA; ΔC: C-terminal deletion mutant) proteins with key regulatory domains (RHD, runt homology domain; NLS, nuclear localization signal; SMID, Smad interaction domain). The ability of the proteins to interact with Smad is indicated to the right of the figure (+, present; −, absent). (*B*) Western blot showing Runx2 and GFP protein levels in PC3 cells infected with lentiviruses containing GFP only, Runx2 WT or mutant Runx2. Runx2 overexpressing cell lines (non-sorted and 2, 3, 4 weeks post sorting) indicate stable Runx2 WT and mutant Runx2 expression. (*C*) Gene expression of WT and mutant Runx2 expressing cell lines 5 weeks post sorting. Expression of Runx2, CSF2 and OPN (osteopontin) mRNA was determined by qPCR. Data were normalized to GAPDH and presented relative to the GFP control. Values are mean ± SEM of n=3 experiments analyzed in duplicate. Statistical analysis (Student's *t*-test) was done by comparing the values of the GFP group with each of the other three groups. *p<0.05, **p<0.01, ***p<0.001.

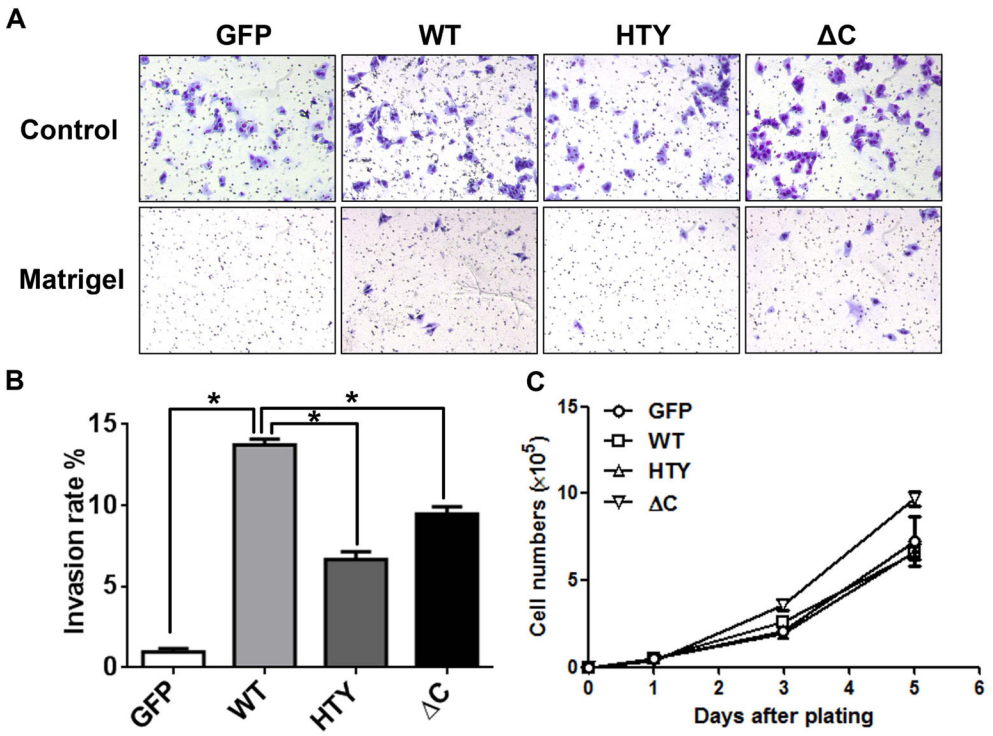

Figure 2.

Runx2 proteins modify phenotypic characteristics of PC3 cells. PC3-L cells expressing GFP, Runx2 WT or Runx2 mutant proteins were subjected to invasion and proliferation assays as described in Materials and Methods. (*A*) Representative images of invasion assays of GFP, Runx2 WT and Runx2 mutant expressing cell lines (HTY and ΔC) are shown. At least three fields of view from each well were photographed (120x). (*B*) Quantitation of invasion assays: percent invasion rates of the GFP, Runx2 WT and Runx2 mutant expressing cell lines are plotted relative to the GFP control. Rates were calculated based on the number of cells that migrated through matrigel and membrane vs. those which migrated through membrane alone (control) (n=3 per group). Student's *t*-test was used to calculate significance by comparing the values of the WT group with the other three groups. *p<0.001. (*C*) Growth curves of the indicated cell lines. Values are mean ± SEM of n=3 experiments analyzed in duplicate. Statistical analysis (Student's *t*-test) was done by comparing values of the GFP group with the other three groups. *p<0.05.

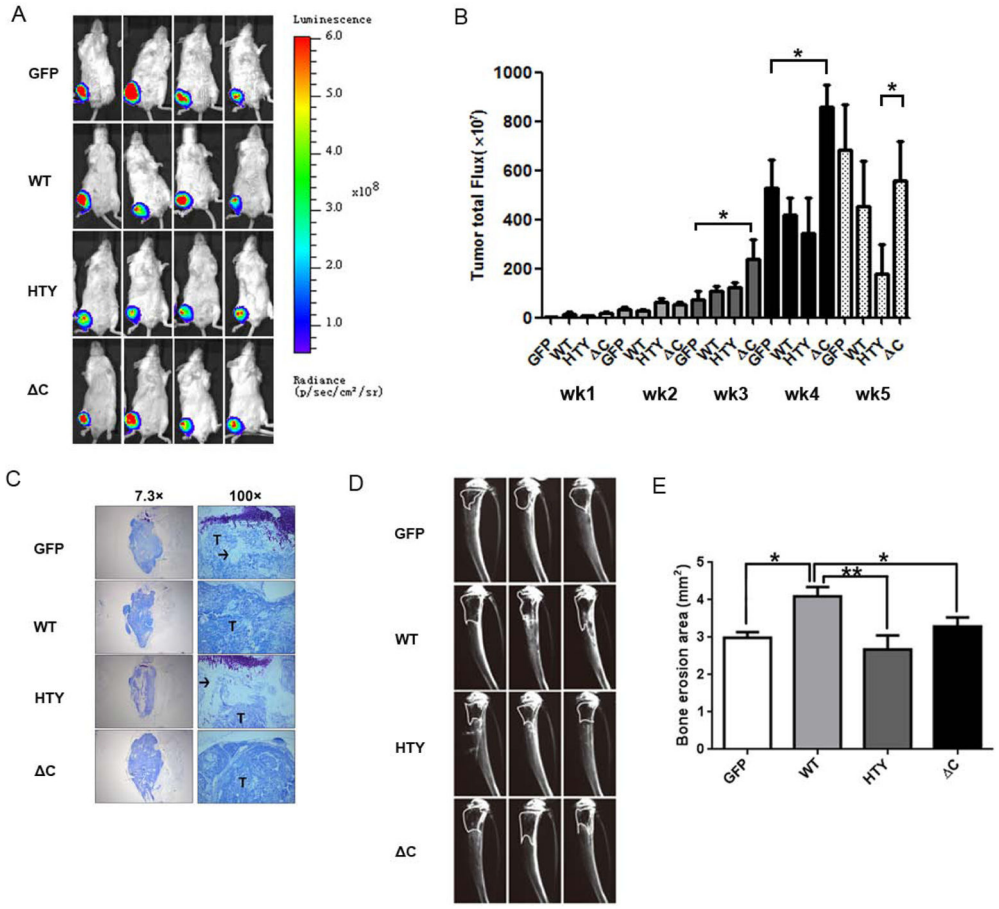

Figure 3.

Intratibial tumor size and associated bone erosion vary according to expression of Runx2 WT or mutants in a xenograft model. (*A*) In vivo imaging of primary tumors. Ventral images of four representative mice (4 of n=6 total) from each group at five weeks post injection are shown. Bioluminescence from the tumors was captured using an IVIS Imaging System. (*B*) Quantification of primary tumor luminescence intensity (corresponding to panel *A*). Images were taken at five time points post-intratibial injection as shown. Values are mean ± S.E.M. for n=6 mice. Statistical analysis (Student's t-test) was done by comparing values of the groups. *p<0.05. (*C*) Representative images of Toluidine blue staining of the intratibial tumors at sacrifice (5 weeks) to show tumor size and extensive loss of trabecular bone in metaphysis and growth plate in epiphysis in WT and ΔC group. (*D*) Representative (3 of n=6 total) radiographs of tumor-bearing tibias 2 weeks after injection with GFP, Runx2 or mutant expressing cell lines. Osteolytic lesions are dark areas outlined with white lines representing loss of trabecular bone. (*E*) Quantification of osteolytic lesions (n=6 mice). Bone erosion areas (as shown in panel *D*) were quantified by ImageJ. Statistical analysis (Student's t-test) was done by comparing values of the WT group with the other three groups.*p<0.05, **p<0.01. Arrow, trabecular bone (white areas); T, tumor.

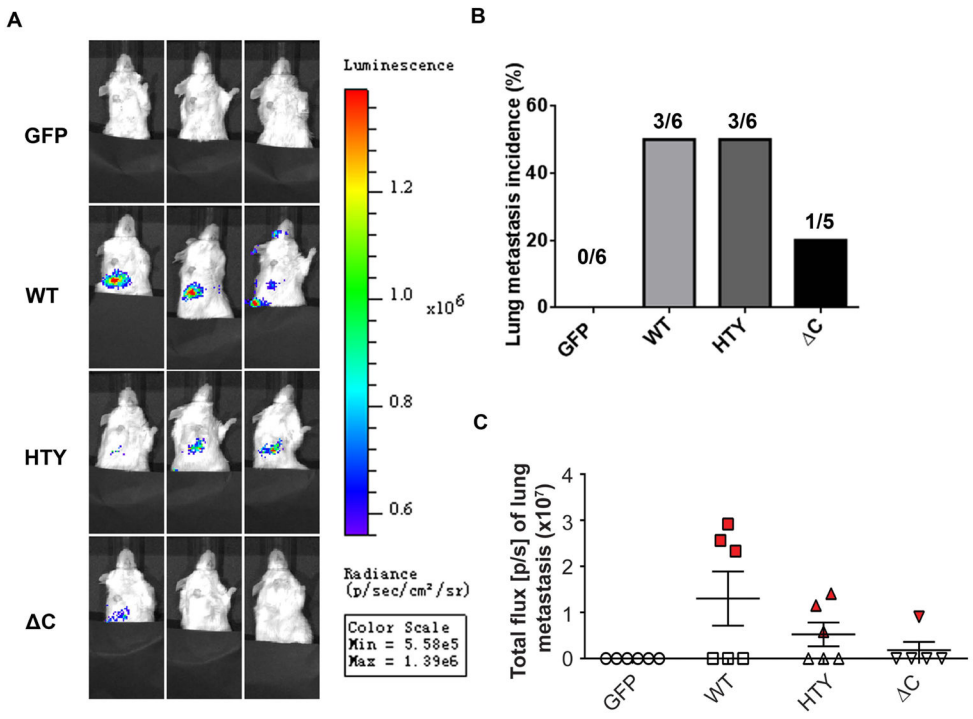

Figure 4.

Runx2 promotes lung metastasis. Mice examined in Fig. 3 for bone tumor growth were also examined by Xenogen imaging for presence of tumor cells in lung. (*A*) Representative images show the extent of lung metastasis in three mice from each group (n=6) 5 weeks after intratibial injection. (*B*) Quantitation of incidence of lung metastasis in GFP, Runx2 WT and Runx2 mutant groups. (n=6, except for n=5 in ΔC group, as indicated). (*C*) Quantitative analysis of metastatic cells in lungs by bioluminescence analysis. Statistical analysis (Student's *t*-test) was done by comparing the values of WT group with the other three groups. *p<0.01.

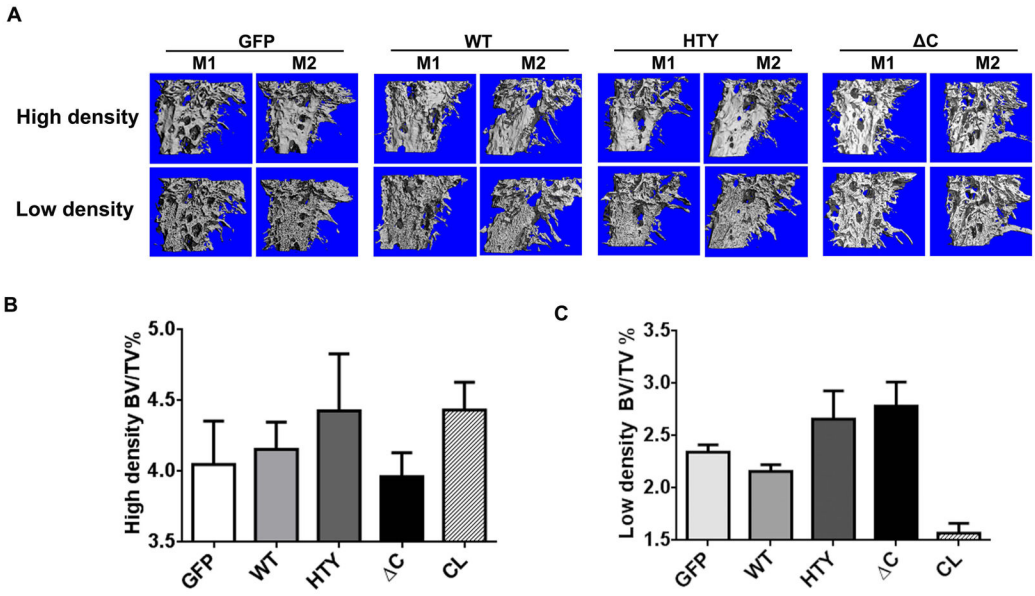

Figure 5.

Overexpression of Runx2 and Runx2 mutant proteins modify bone mass in tumor bearing tibias. (*A*) Two representative micro-CT images of high bone density in tumor-bearing tibias are shown for each group (GFP, WT, HTY and ΔC) at five weeks post-injection by micro-CT. Osteolytic areas are indicated by empty regions in solid bone; mostly mature woven bone is visualized as fine bony projections from the cortical bone. M=mouse. (*B*), (*C*) Quantitative micro-CT analysis of high density bone volume fraction (*B*) and low density bone volume fraction (*C*) of tumor-bearing tibias. Total volume (TV) is the same in each group. *ANOVA analysis was performed by comparing the values of all the groups. p=0.05. *The contralateral limb CCL is shown for reference to normal bone

A

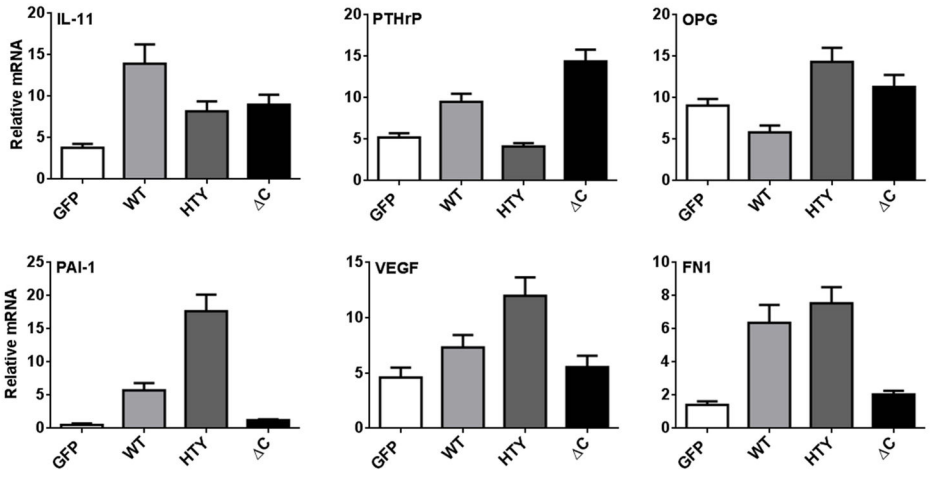

B

Genes	IL-11	PTHrP	OPG	PAI-1	VEGF	FN1
GFP [a] vs. WT [b]	1.7×10^{-4}	3×10^{-3}	0.03	2.9×10^{-7}	NS	0.01
GFP [a] vs. HTY [c]	4×10^{-3}	NS	0.03	2.8×10^{-8}	0.03	7×10^{-3}
GFP [a] vs. ΔC [d]	2×10^{-3}	1.2×10^{-4}	NS	8×10^{-5}	NS	NS
WT [b] vs. ΔC [d]	NS	0.02	5×10^{-3}	3.7×10^{-5}	NS	0.02
WT [b] vs. HTY [c]	0.03	4.4×10^{-4}	7.3×10^{-4}	5.9×10^{-4}	NS	NS
HTY [c] vs. ΔC [d]	NS	2.7×10^{-5}	NS	8×10^{-7}	3×10^{-3}	0.02

[a] GFP control; [b] Runx2 wild-type; [c] Runx2 HTY mutant; [d] Runx2 ΔC mutant

C

Figure 6.

Disruption of Runx2-Smad interaction (HTY) and deletion of the Runx2 C-terminus (ΔC) result in altered expression of metastasis-related genes. Adenovirus infected cancer cells expressing Runx2 protein showing changes in molecular markers of osteolytic genes was validated in earlier *in vitro* studies.[11] (*A*) The relative expression of Runx2 target genes (IL-11, PTHrP, OPG (osteoprotegrin), PAI-1, VEGF, and FN1) in response to Runx2 WT and mutant protein overexpression is shown. All data were normalized to GAPDH. Values are mean ± SEM of n=3 experiments analyzed in duplicate. ANOVA analysis was done by comparing the values of all four groups. Statistical results are shown in Table S2. (*B*) The relationship between changes in gene expression and tumor properties in the Runx2 mutant groups compared to Runx2-WT. Arrows indicate up- and down-regulation of the six most highly expressed genes. BR=bone resorption; TG=tumor growth.